Geophysical Research Letters

RESEARCH LETTER
10.1029/2022GL102087

Evaluating Satellite Precipitation Estimates Over Oceans Using Passive Aquatic Listeners

J. L. Bytheway[1,2], E. J. Thompson[2], J. Yang[3], and H. Chen[4]

[1]Cooperative Institute for Research in Environmental Sciences, University of Colorado Boulder, Boulder, CO, USA, [2]NOAA Physical Sciences Laboratory, Boulder, CO, USA, [3]Applied Physics Lab, University of Washington, Seattle, WA, USA, [4]Department of Electrical Engineering, Colorado State University, Fort Collins, CO, USA

Key Points:

- Passive aquatic listeners provide useful 5 km areal oceanic precipitation estimates to validate satellite products at similar spatial grids
- Satellite-based precipitation estimates compare more favorably to passive aquatic listener observations with increasing time scale
- Satellite-based precipitation estimates perform better in extratropical oceans than tropical oceans

Correspondence to:

J. L. Bytheway,
janice.bytheway@noaa.gov

Citation:

Bytheway, J. L., Thompson, E. J., Yang, J., & Chen, H. (2023). Evaluating satellite precipitation estimates over oceans using passive aquatic listeners. *Geophysical Research Letters*, *50*, e2022GL102087. https://doi.org/10.1029/2022GL102087

Received 15 NOV 2022
Accepted 27 JAN 2023

Abstract Passive aquatic listeners (PALs) provide high-quality, high-resolution estimates of precipitation over ocean regions, but have been underutilized as a reference data set for the evaluation of satellite-based precipitation estimates (SPEs). PALs are uniquely suited for this purpose due to their 5 km surface listening area when sampling at 1 km depth on drifting Argo Floats, providing rain rate estimates on a spatial scale similar to the native grid spacing of many SPEs. In this study we compare three SPE products (IMERG, CMORPH, and PDIR-Now) to PAL measurements. Evaluations are performed over tropical, extratropical, and global oceans at SPE native spatiotemporal resolution and longer time scales. We find the SPEs to have rain rate frequency distributions similar to PAL, but with biases and varying performance characteristics that are dependent on region and time scale.

Plain Language Summary Satellites are the only source of precipitation observations that cover the entire global oceans, but it is difficult to quantify the accuracy of these measurements because of there are not many surface-based observations, such as rain gauges, to compare them to. Rain gauges over the ocean are mounted on stationary buoys and only provide information over a small fraction of the ocean area. The Passive Aquatic Listener (PAL) is an instrument that is mounted on a platform that drifts with ocean currents at a depth of 1 km, and uses recorded sound waves to estimate rain rate at the ocean surface. PAL observations are made at a time and space scale that is similar to that of satellite-based precipitation products, and because the instruments drift with ocean currents they can cover more ocean area than a stationary buoy. PAL data was recently reprocessed and made available for use, and this study represents the first use of PAL observations to evaluate three satellite-based precipitation products over the global oceans. In general, satellite-based precipitation estimates compare best to the PAL when averaged over multiple hours or an entire day, and their performance is different in tropical and extra-tropical ocean regions.

1. Introduction

Over 75% of global rainfall occurs over the ocean (Trenberth et al., 2007), and this precipitation plays an important role in the surface freshwater flux, upper ocean salinity, and upper ocean stability (Prakash et al., 2012; Ramesh Kumar & Schulz, 2002). Understanding the accuracy and utility of satellite-based precipitation estimates (SPEs) over oceans is necessary to advance our ability to monitor and predict variations in the global energy and hydrologic cycles that drive weather and climate. For example, precipitation-induced buoyancy fluxes impact vertical ocean density gradients and ocean mixed layer salinity structure, in turn suppressing ocean turbulence and influencing ocean circulations and heat content (Kucera & Klepp, 2022; Yang et al., 2015). Depending on the rain rate (RR) intensity relative to surface stress and cooling, impacts of freshwater flux on the ocean surface can last for hours to days (Asher et al., 2014; Drushka et al., 2016; Reverdin et al., 2020; Thompson et al., 2019), and can contribute to the formation of larger-scale, ∼10–50 m depth barrier layers that last weeks to months (Drushka et al., 2012; Lukas & Lindstrom, 1991; Sprintall & Tomczak, 1992). Additionally, rain, particularly in the tropics, can cool the ocean surface, inducing a sensible heat flux to the atmosphere on the order of 50–200 W m^{-2} that influences both sea surface and air temperature (Gosnell et al., 1995).

Validating SPEs over ocean is challenging because operational in-situ measurements of oceanic precipitation are generally limited to gauges on a relatively small number of moored buoys and research vessels, most of which are in relatively high-precipitation tropical regions (Maggioni et al., 2016; Prakash et al., 2018; Sapiano & Arkin, 2009; Wu & Wang, 2019). These gauges are susceptible to undercatch due to wind, platform motion,

turbulence around the ship structure, intermittent data outages, and vandalism (Kucera & Klepp, 2022; Maggioni et al., 2016; Wu & Wang, 2019; Yang et al., 2015). Observations from the Ocean Rainfall And Ice-phase precipitation measurement Network (OceanRAIN) aim to overcome the shortcomings of gauges by measuring precipitation with optical disdrometers on eight ships that traversed the global oceans from June 2010 through December 2018 (Klepp, 2015; Klepp et al., 2018; Kucera & Klepp, 2022), thus providing more geographic coverage than stationary moored buoys. Recently, 12 years of research-based observations from passive aquatic listeners (PALs) – hydrophones capable of detecting the unique frequency of raindrops falling with different intensities on the ocean surface – were reprocessed and made available for use (Yang et al., 2015). Since 2011, 58 PALs have been deployed on moorings and drifting Argo floats, however their data has not been widely used outside of field campaigns.

Satellite-based precipitation estimates can provide near-global RR estimates at relatively high spatial and temporal resolution. Such products typically combine retrievals from multiple satellites, often combined with motion vectors and bias correction using in situ measurements. While many studies have sought to validate SPEs over ocean (e.g., Kucera & Klepp, 2022; Maggioni et al., 2016; Prakash et al., 2018; Wu & Wang, 2019), this evaluation remains less comprehensive than over land due to the sparseness of in-situ measurements. Surface-based radars located on islands or near coastlines can somewhat increase the data availability for oceanic validation of SPE, however coastal transitions can introduce artifacts in satellite precipitation retrievals (Carr et al., 2015; Derin et al., 2021; Wolff & Fisher, 2008). Ship-based radars have also been deployed but typically have short data records (∼1 month).

Understanding the performance of SPEs over the ocean can help improve our understanding of the role precipitation plays in global air-sea interaction, physical oceanography, and the coupled weather and climate system. Here, we evaluate the performance of several SPEs using in-situ PAL measurements. Like many in-situ oceanic observation networks, the PALs provide high temporal resolution RR estimates but represent only a small portion of the vast ocean surface. Unlike other point-based observations, RR retrieved from PALs have a spatial footprint similar to the native resolution of gridded SPEs (∼5 km).

2. Data

2.1. Passive Aquatic Listeners

PALs have been deployed on drifting Argo floats (Riser et al., 2008; Roemmich et al., 2019) and stationary moorings across the global oceans. The PAL records an ambient noise time series which is converted to a frequency spectrum over 1–50 kHz, where the dominant noise sources are rain, wind, and anthropogenic sources like shipping and oil drilling. Multivariate analysis using sound pressure levels (SPL) at multiple frequencies combined with the slope between SPLs at different frequencies is used to classify the distinctive sound source (for details, see Yang et al., 2015). For each ambient noise data point, classification and estimation is exclusive, that is, data classified as “rain” is only used to estimate RR while those classified as “wind only” are only used to estimate wind speed. This rule is designed to ensure good estimation of wind speed since rain noise may overwhelm the noise level generated by wind. Both RR and wind speed estimates from PALs mounted on stationary moorings have been compared to co-located surface rain and wind speed observations, with favorable results demonstrating the fidelity of the PAL-based RR and wind speed estimates (Ma & Nystuen, 2005; Nystuen, 2001; Yang et al., 2015).

Argo floats drift with surrounding ocean currents, remaining at 1-km depth for approximately 9 days between each vertical profile and surface data telemetering period. While drifting at depth, PALs record data every 2–9 min depending on classification results (classification of current data point as drizzle, heavy rain, or wind determines whether the next sample will be recorded at a 4, 2, or 8 min interval, respectively). The circular surface listening area sampled by PAL has diameter approximately five times its depth, resulting in a 5 km surface footprint for PALs drifting at 1 km depth. PALs on moorings have been deployed at variable depths, however only those deployed at 1 km depth are considered in this study. The PAL's sampling strategy provides a spatial resolution ideal for comparison with high resolution gridded SPEs, which have grid spacing <=10 km every 0.5–1 hr. The archive of PAL wind speed and rain rate data from 2011-present was recently reprocessed in NetCDF format with uniform 1-min time steps and linearly interpolated float location between Global Positioning System (GPS) fixes (Thompson et al., 2023).

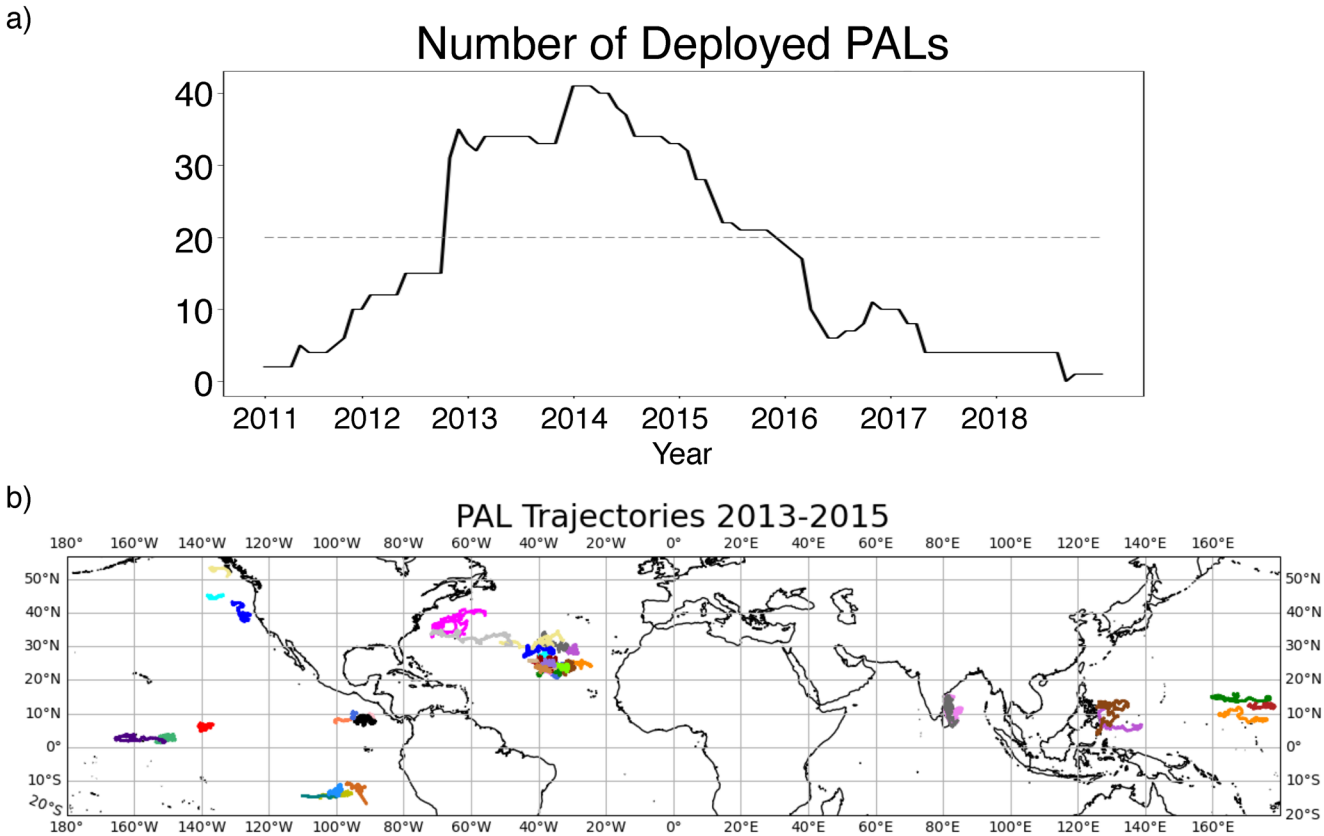

Figure 1. (a) Number of PALs deployed monthly from 2011 through 2018. Gray dashed line denotes $n = 20$. (b) Location of PALs deployed from 2013 to 2015 that are used in this study. Different colors are used for each PAL to aid visibility.

PALs have been deployed as part of field campaigns including Aquarius, two National Aeronautics and Space Administration (NASA) Salinity Processes in the Upper Ocean Regional Study (SPURS) campaigns (Bingham et al., 2019; Lindstrom et al., 2017, 2019), and National Oceanic and Atmospheric Administration (NOAA) Tropical Pacific Observing System (TPOS). PALs remain deployed for a period of 1–4 years, so the number of PALs available at any given time is highly variable. Figure 1a shows the monthly count of deployed PALs from 2011 to 2018. The availability of PAL data peaks in 2013–2015, corresponding to the SPURS-1 campaign in the tropical Atlantic Ocean. Figure 1b shows the trajectory of PALS during this period. While the coverage of the PALs is mostly limited to the Northern Hemisphere tropics, they are also found in the tropical Southern Pacific Ocean and off both coasts of North America. Because of the relatively large number of available pals (20+) and quasi-global coverage, we focus our evaluation on the period 2013–2015.

2.2. Satellite-Based Precipitation Estimates

Three SPEs are evaluated in this study. The Climate Prediction Center (CPC) Morphing Technique (CMORPH) and Integrated Multi-satellitE Retrievals for Global Precipitation Measurement (IMERG) algorithms mainly use observations from passive microwave (PMW) radiometers on low earth orbiting (LEO) satellites, while the Precipitation Estimation from Remotely Sensed Information Using Artificial Neural Networks (PERSIANN)—Dynamic Infrared Rain Rate (PDIR-Now) product uses only infrared brightness temperature (Tb) measurements from Geostationary satellites (GEO-IR).

2.2.1. CMORPH V1.0

The CMORPH precipitation product (Xie et al., 2019) is available globally at 30-min time steps with 8 km grid spacing. CMORPH uses retrieved instantaneous RR from PMW radiometers on LEO satellites combined with cloud motion vectors derived from GEO-IR satellite imagery. In the "morphing" technique, retrieved RR from the PMW is interpolated both forwards and backwards in time using the derived motion vectors to determine the shape and

location of precipitation features in between LEO overpasses (Joyce et al., 2004). CPC daily gauge analysis is used to bias-correct the multisensor RR over land, while probability density function (PDF) matching against monthly precipitation analysis from the Global Precipitation Climatology Project (GPCP) is performed over ocean (Xie et al., 2017). Full descriptions of the CMORPH algorithm and products are given in Joyce et al. (2004) and Xie et al. (2017).

2.2.2. IMERG V6 Final

IMERG (Huffman, Bolvin, et al., 2019; Huffman, Stocker, et al., 2019) is available globally at 0.1° grid spacing (approximately 10 km) and 30 min temporal resolution. Like CMORPH, IMERG interpolates RR from PMW satellites in time and space using motion vectors between individual LEO satellite overpasses. IMERG includes intercalibration of the PMW-based RR estimates to help reduce uncertainties due to slight sensor differences among the PMW constellation. Motion vectors are derived from numerically modeled total precipitable water vapor fields. Additionally, PMW-calibrated IR-based precipitation estimates from the PERSIANN Cloud Classification System (CCS) are incorporated using the CMORPH-Kalman Filter (Tan et al., 2019). While monthly gauge data from various sources is used to reduce biases over land (Huffman, Bolvin, et al., 2019; Huffman, Stocker, et al., 2019), no gauge-based bias correction is performed over ocean due to the scarcity of available observations. Three versions of IMERG are available with varying latency: IMERG Early, IMERG Late, and IMERG Final. IMERG Final includes the most available PMW retrievals and bias correction so is selected here for analysis.

2.2.3. PDIR-Now

The PDIR-Now data set is the most recent high-resolution, low-latency PERSIANN precipitation product, providing hourly quasi-global (60°N-S) RR at 0.04° (approximately 4 km) grid spacing. Unlike IMERG and CMORPH, RR from PDIR-Now is based only on observations from GEO-IR. PDIR-Now surface RR estimates use relationships between IR Tbs and RR that are calculated by a neural network trained on IMERG Merged PMW-only RR retrievals. The Tb-RR relationships are further refined using precipitation climatologies from Worldclim2 and PERSIANN-Climate Data Record over land and ocean, respectively. Full details of PDIR-Now can be found in Nguyen, Shearer et al. (2020) and Nguyen, Ombadi, et al. (2020).

3. Methods

PAL's minute-scale RR were averaged to 0.5, 1, 6, and 24 hr for comparison to the SPEs at their native resolutions and these longer timescales. Previous studies (Tan et al., 2017; Wu & Wang, 2019) have shown that SPEs, particularly IMERG, compare more favorably with in-situ surface measurements when averaged to larger spatiotemporal scales. While PAL point measurements cannot be aggregated to coarser spatial resolution, we do perform comparisons at coarser temporal resolution.

SPE products are matched to the average latitude and longitude of the PAL over the averaging period. The PALs do not move more than 3 km per day in O 1 cm/s speed 1-km depth ocean currents, and so would not be expected to traverse multiple SPE grid boxes over the course of a day (Ollitrault and de Verdière, 2014).

We perform a number of direct comparisons and calculate several evaluation metrics on the temporally-averaged PAL-SPE spatial matches. Contingency table statistics (Probability of detection, POD, False alarm ratio, FAR, and Heidke Skill Score, HSS) are calculated using scaled detection thresholds obtained using Equation 1 from Tan et al. (2017) using a spatial resolution of 0.1° (the coarsest among the SPEs). This results in threshold values of 0.2, 0.14, 0.06, and 0.03 mm h^{-1} corresponding to 0.5, 1, 6, and 24 hr average RR, respectively. Calculating the thresholds using the lowest spatial resolution between the SPE and PAL results in the lowest, or most conservative, thresholds for detection. Bias is calculated conditionally; that is, bias is only calculated when both SPE and PALs indicate the presence of precipitation. To isolate latitude belts and thus rain regimes, we define the tropics as being equatorward of 30°N/S and extratropics as poleward of 30°N/S. Additionally, because PMW-based SPEs are known to struggle with frozen precipitation (Levizzani et al., 2011; Skofronick-Jackson et al., 2013), we also perform evaluations in the extratropics during the warm season only (boreal May–Oct).

4. Results

4.1. Comparing SPE With PAL

Figure 2 compares the distribution of RR from the various SPE products by showing CDFs of average RR from SPEs and PALs at PAL locations at 0.5, 1, 6, and 24 hr time periods. The difference between the CDFs of SPEs and

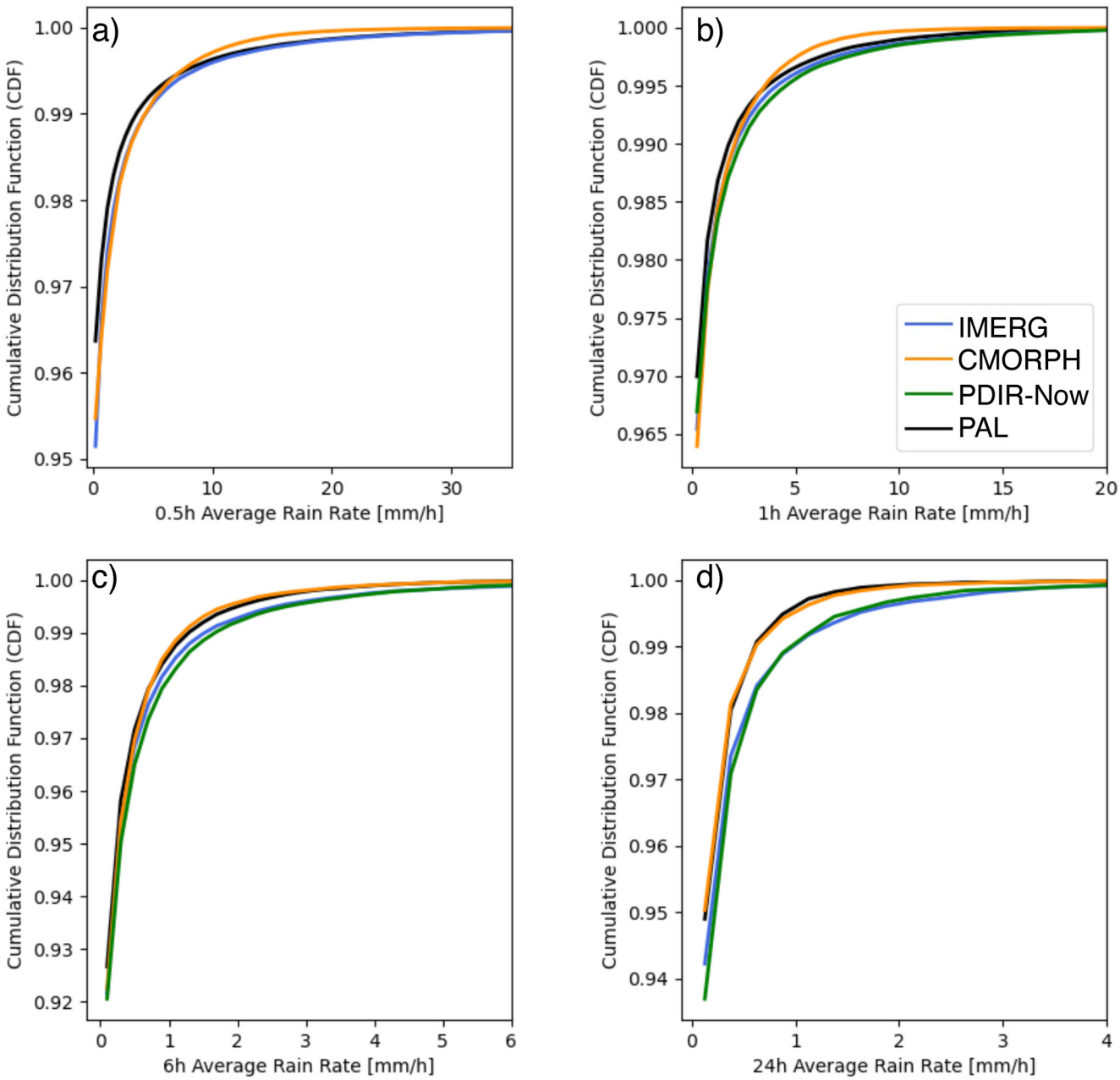

Figure 2. CDFs of mean RR over the global ocean from PAL, IMERG, CMORPH, and PDIR-Now at (a) 0.5 hr, (b) 1 hr, (c) 6 hr, and (d) 24hr.

the PAL measurements is small, on the order of less than 1% for all RR values. At the highest temporal resolution (0.5 hr, Figure 2a), IMERG and PAL distributions for RR > 10 mm°hr^{-1} are in very close agreement, while IMERG and CMORPH have similar distributions at lower RR. For 1 hr RR (Figure 2b), CMORPH has fewer occurrences of RR > 5 mm/hr, while IMERG and PDIR-Now CDFs are slightly below the PAL distribution for all RR. As temporal averaging increases and therefore the average hourly RR over longer time periods decreases, CMORPH distributions show a better match to the PAL distribution at 6 and 24 hr (Figures 2c and 2d). IMERG and PDIR-Now CDFs remain similar to each other, both having a smaller occurrence of low RR than PAL and CMORPH, and having higher occurrence of slightly higher average RR. The monthly GPCP bias correction may be contributing to differences between the CMORPH CDFs and those from the unadjusted IMERG and PDIR-Now products.

Figure 3 shows average annual rainfall accumulations at PAL locations for each of the 3 years studied for global, tropical, and extratropical oceans (solid, dashed, and dotted lines, respectively). Since the majority of the PALs

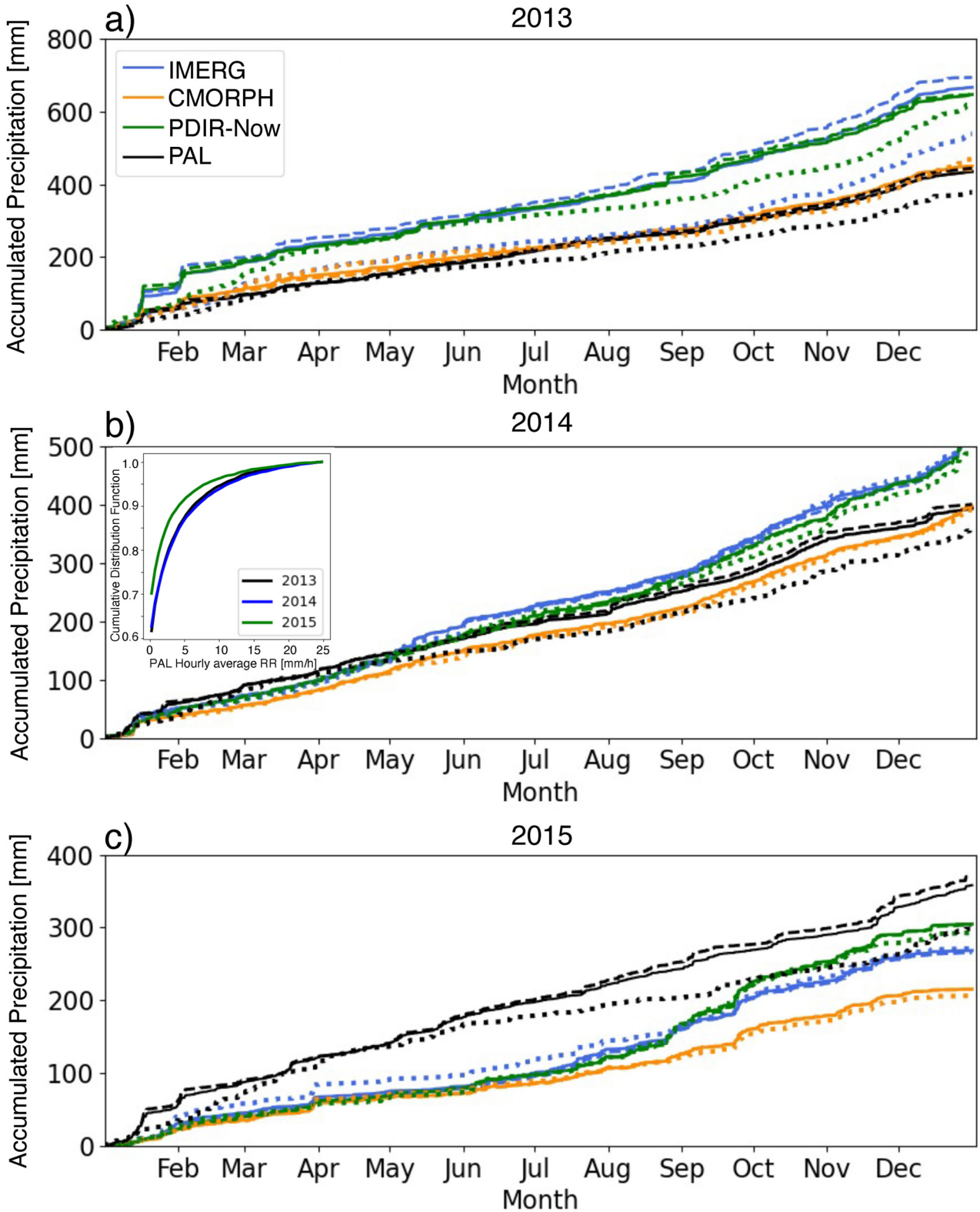

Figure 3. Average annual precipitation accumulation at PAL locations for (a) 2013, (b) 2014, and (c) 2015 over global (solid), tropical (dashed) and extratropical (dotted) oceans. Inset of (b) shows CDFs of PAL hourly RR over global oceans for each year.

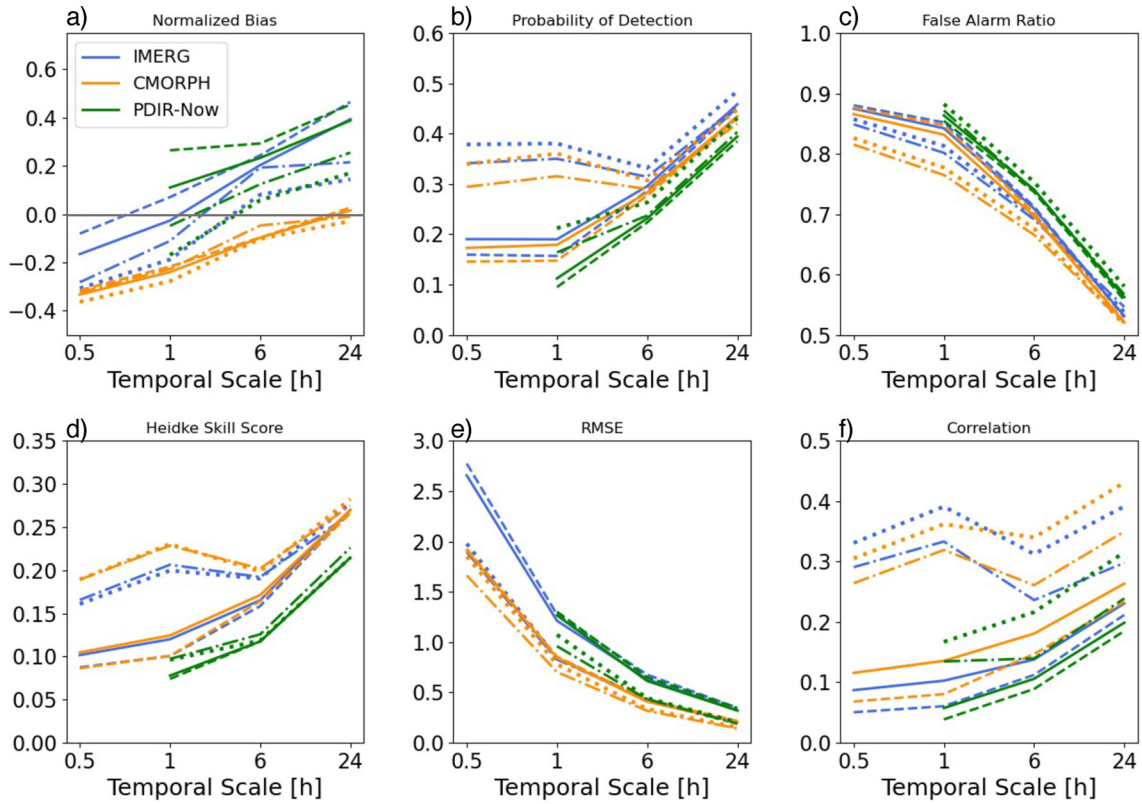

Figure 4. Evaluation statistics for IMERG (blue), CMORPH (orange), and PDIR-Now (green) compared to PAL at 0.5, 1, 6, and 24 hr. (a) Normalized Bias, (b) POD, (c) FAR, (d) HSS, (e) RMSE, and (f) Correlation Coefficient. Statistics are calculated over global oceans (solid), tropical oceans (dashed), extratropical oceans (dotted), and extratropical warm season (May-Oct) only (dash-dotted).

are located in tropical oceans, the average accumulation over global oceans is strongly related to the average accumulated precipitation at tropical PAL locations. In 2013 and 2014 (Figures 3a and 3b), IMERG and PDIR-Now largely overestimated precipitation at PAL locations in all three ocean domains. CMORPH agrees with PAL values fairly well in 2013 for global and tropical average precipitation, and slightly underestimates tropical average precipitation in 2014. Extratropical average precipitation from CMORPH in both 2013 and 2014 is slightly overestimated. In 2015 (Figure 3c), all three SPEs underestimated precipitation at PAL locations both globally and in the sub-basins, with the exception of PDIR-Now in the extratropics starting in October. This difference in SPE behavior in 2015 versus 2013 and 2014 is hypothesized to be related to the presence of a strong El Nino that began in spring of 2015, whereas 2013 and 2014 were both ENSO Neutral years. This is supported by CDFs of rain rate in 2015 that have less frequent non-zero precipitation and fewer high RRs than those in 2013 and 2014 (Figure 3b inset) and follows previous research that indicated SPE performance is related to the characteristics of the precipitation itself (Adhikari et al., 2019; Guilloteau et al., 2018; Petkovic et al., 2019).

4.2. Evaluation Metrics

Figure 4 shows several standard verification metrics calculated for the SPEs using PALs as the reference. Compared to the global oceans, both IMERG and PDIR-Now have larger magnitude biases in the tropics at all temporal resolutions (except 0.5 hr for IMERG), while bias magnitudes for CMORPH are similar in all locations (Figure 4a). Conditional biases in the extratropics are lower, but not necessarily better, than global and tropical biases (i.e., less positive high biases, but more negative low biases). These extratropical low biases seem to be driving the global low bias values at 0.5 and 1 hr periods in IMERG, and also moderating the high bias PDIR-Now exhibits in the tropics to produce a lower positive value over the global oceans.

POD increases with increasing temporal scale (Figure 4b), but the manner of increase is regionally dependent. In the global and tropical oceans, there is a sharp increase in values starting at 1 hr, while the extratropical oceans have similar values at 0.5, 1, and 6 hr, with a large increase at 24 hr. Somewhat surprising is the slight decrease

in POD in the extratropics at 6 hr for both IMERG and CMORPH. IMERG displays the highest POD of all SPEs for all temporal scales and regions, while CMORPH has only slightly lower values. POD for all SPEs is highest in the extratropics, and lowest in the tropics, with smaller differences between the regions at 6 and 24 hr. POD during the extratropical warm season is slightly lower than year-round.

Smaller variations are noted between SPEs for FAR (Figure 4c) than for POD, with decreasing variations in statistics between products or between regions at larger temporal scales. FAR at hourly and half-hourly scales is quite high, and decreases sharply with increasing temporal scale. IMERG and CMORPH FAR are fairly similar globally and in the tropics, with IMERG having somewhat higher FAR than CMORPH. There are slightly larger variations in FAR between the products in the extratropics. While FAR is highest for CMORPH and IMERG in the tropics, PDIR-Now has the highest FAR in the extratropics. PDIR-Now also exhibits the smallest regional variations in FAR at all temporal scales.

HSS is low for all SPEs (Figure 4d), with CMORPH having a higher HSS than IMERG in the extratropics at sub-daily scales, and CMORPH and IMERG having more similar values at daily scale in all regions. Regional differences between SPEs for all statistics are largest at higher temporal resolution. Like POD, HSS also shows a slight unexplained decrease in skill for the PMW-based SPEs in the extratropics at 6 hr.

Root Mean Square Error (RMSE, Figure 4e) decreases with increasing temporal scale for all SPEs. IMERG exhibits the highest RMSE values, with PDIR-Now having similar RMSE values to IMERG except at hourly scales in the extratropics, where PDIR-Now has slightly higher RMSE than IMERG. CMORPH has the lowest RMSE values at all temporal scales, and also exhibits the smallest variations in RMSE between ocean regions compared to the other SPEs. For all of the SPEs, correlation coefficients (Figure 4f) in the extratropics are much higher than in the tropics or globally, and within the extratropical oceans, the year-round values are higher than those during the warm season only. In the extratropics, the PMW-based SPEs again indicate a slight degradation in performance at 6 hr RR, while in the tropical and global oceans correlation coefficient increases steadily with increasing temporal scale.

5. Discussion and Conclusions

To our knowledge, this study represents the most comprehensive comparison of PAL RR measurements to SPEs over oceans. SPEs continue to be a key source of oceanic precipitation information; however, our understanding of their performance for this purpose is limited by insufficient in-situ observations. While the PALs are prone to many of the same issues as existing oceanic precipitation observations (e.g., relatively low spatial coverage and thus large sampling bias, bias toward tropical placement), they have several advantages that can help increase our understanding of SPE performance over ocean. First is the 5 km spatial footprint of the PAL when drifting at a depth of 1 km which is similar in size to the grid spacing of SPE products. Thus, PAL and SPE data are relatable areal precipitation estimates. Second, the deployment of PALs on drifting Argo floats allows for some evaluation of SPEs in oceanic regions not previously covered by field campaigns or moorings.

SPEs compared more favorably to PALs when data were averaged to coarser temporal resolution (e.g., >=6 hr), consistent with previous studies. Numerically, normalized bias values for all SPE products increased with increasing temporal scale. For the PMW-based products, this increase in bias involved a change in sign from low bias at high temporal resolution to slight positive bias at longer timescales, while PDIR-Now biases were positive everywhere except at 1 hr in the extratropics. Because we considered the conditional bias, we hypothesize that biases are more positive in the tropics due to the SPEs correctly identifying deep organized convection but overestimating RR. In the extratropics, where lighter stratiform precipitation is more common, we hypothesize that the larger spatial extent of precipitating systems results in a higher likelihood of precipitation being detected, but that weak ice scattering signals in the PMW retrieval algorithms results in lower retrieved RR than observed, and thus low biases. This notion is supported by the contrast in low tropical POD and higher extratropical POD at high temporal resolution. CMORPH, on the other hand, consistently underestimates at all but daily temporal scales. The cause for this, as well as the explanation for why the PMW SPEs have degraded validation statistics at 6 hr temporal scale versus 1 hr are unclear.

Potential uncertainties in the reference data set may also impact the evaluation results. In this case, we specifically note that the linear interpolation of PAL geolocation in between surface location fixes introduces small uncertainties in the location of the PAL at a given time. To test the possibility of SPE-to-PAL location mismatch, the analysis was repeated using the neighborhood maximum (NM) technique (Schwartz, 2017) on all SPE grid boxes

surrounding the box containing the PAL at a given time. This approach yielded the same or slightly degraded results from those shown in Section 4, and therefore we conclude that location mismatch between the SPE and PAL is likely not a large source of uncertainty in the results.

While both CMORPH and IMERG are predominantly based on retrieved RR from PMW observations, PDIR-Now is IR-only. As such, comparing PDIR-Now performance to that of the PMW-based products is not an "apples-to-apples" comparison. Finally, although PAL data used in this study contains observations in both the tropical and extratropical oceans, there is far more PAL data available in the tropics, which tend to dominate the global ocean results.

Data Availability Statement

CMORPH Version 1.0 30 min 8 km data can be obtained from the National Centers for Environmental Information (NCEI) at https://doi.org/10.25921/w9va-q159. IMERG V6 was obtained via NASA Earthdata Search: https://search.earthdata.nasa.gov/search?q=GPM_3IMERGHH_06 (requires registration). PDIR-Now is available from the Center for Hydrometeorology and Remote Sensing (CHRS) Data Portal at https://chrsdata.eng.uci.edu/. PAL data is archived at NASA (https://doi.org/10.5067/GPMGV/PAL/DATA101).

Acknowledgments
All authors acknowledge NASA Precipitation Measurement Mission Grant 18-PMMST18-0018, interagency agreement 80HQTR20T0049, led by EJT, for support of this project. Additionally, EJT was supported by the NOAA Physical Sciences Laboratory. JLB was also supported by NOAA Cooperative Agreements NA17OAR4320101 and NA22OAR4320151.

References

Adhikari, A., Liu, C., & Hayden, L. (2019). Uncertainties of GPM Microwave Imager precipitation estimates related to precipitation system size and intensity. *Journal of Hydrometeorology*, *20*(9), 1907–1923. https://doi.org/10.1175/JHM-D-19-0038.1

Asher, W. E., Jessup, A. T., Branch, R., & Clark, D. (2014). Observations of rain-induced near-surface salinity anomalies. *Journal of Geophysical Research: Oceans*, *119*(8), 5483–5500. https://doi.org/10.1002/2014JC009954

Bingham, F. M., Tsontos, V., de Charon, A., Lauter, C. J., & Taylor, L. (2019). The SPURS-2 Eastern Tropical Pacific field campaign data collection. *Oceanography*, *32*(2), 142–149. https://doi.org/10.5670/oceanog.2019.222

Carr, N., Kirstetter, P.-E., Hong, Y., Gourley, J. J., Schwaller, M., Petersen, W., et al. (2015). The influence of surface and precipitation characteristics on TRMM Microwave imager rainfall retrieval uncertainty. *Journal of Hydrometeorology*, *16*(4), 1596–1614. https://doi.org/10.1175/JHM-D-14-0194.1

Derin, Y., Kirstetter, P.-E., & Gourley, J. J. (2021). Evaluation of IMERG satellite precipitation over the land-coast-ocean continuum. Part I: Detection. *Journal of Hydrometeorology*, *22*, 2843–2859. https://doi.org/10.1175/JHM-D-21-0058.1

Drushka, K., Asher, W. E., Ward, B., & Walesby, K. (2016). Understanding the formation and evolution of rain-formed fresh lenses at the ocean surface. *Journal of Geophysical Research: Oceans*, *121*(4), 2673–2689. https://doi.org/10.1002/2015JC011527

Drushka, K., Sprintall, J., Gille, S. T., & Wijffels, S. (2012). In situ observations of Madden– Julian Oscillation mixed layer dynamics in the Indian and Western Pacific Oceans. *Journal of Climate*, *25*(7), 2306–2328. https://doi.org/10.1175/JCLI-D-11-00203.1

Gosnell, R., Fairall, C. W., & Webster, P. J. (1995). The sensible heat of rainfall in the tropical ocean. *Journal of Geophysical Research*, *100*(C9), 18437–18442. https://doi.org/10.1029/95JC01833

Guilloteau, C., Foufoula-Georgiou, E., Kummerow, C. D., & Petkovic, V. (2018). Resolving surface rain from GMI high-frequency channels: Limits imposed by the three-dimensional structure of precipitation. *Journal of Atmospheric and Oceanic Technology*, *35*(9), 1835–1847. https://doi.org/10.1175/JTECH-D-18-0011.1

Huffman, G. J., Bolvin, D. T., Braithwaite, D., Hsu, K., Joyce, R., Kidd, C., et al. (2019). NASA global precipitation measurement (GPM) integrated multi-satellitE retrievals for GPM (IMERG). Algorithm theoretical basis doc., version 06 (p. 38). Retrieved from https://docserver.gesdisc.eosdis.nasa.gov/public/project/GPM/IMERG_ATBD_V06.pdf

Huffman, G. J., Stocker, E. F., Bolvin, D. T., Nelkin, E. J., & Tan, J. (2019). GPM IMERG final precipitation L3 half hourly 0.1 degree x 0.1 degree V06, Greenbelt, MD, Goddard Earth Sciences data and information services center (GES DISC). https://doi.org/10.5067/GPM/IMERG/3B-HH/06

Joyce, R. J., Janowiak, J. E., Arkin, P. A., & Xie, P. (2004). CMORPH: A method that produces global precipitation estimates from passive microwave and infrared data at high spatial and temporal resolution. *Journal of Hydrometeorology*, *5*(3), 487–503. https://doi.org/10.1175/1525-7541(2004)005,0487:CAMTPG.2.0.CO;2

Klepp, C. (2015). The oceanic shipboard precipitation measurement network for surface validation - OceanRAIN. *Atmospheric Research*, *163*, 74–90. https://doi.org/10.1016/j.atmosres.2014.12.014

Klepp, C., Michel, S., Protat, A., Burdanowitz, J., Albern, N., Kahnert, M., et al. (2018). OceanRAIN, a new in-situ shipboard global ocean surface-reference dataset of all water cycle components. *Scientific Data*, *5*(1), 180122. https://doi.org/10.1038/sdata.2018.122

Kucera, P. A., & Klepp, C. (2022). Evaluation of high-resolution satellite precipitation over the global oceans. In S. Michaelides (Ed.), *Precipitation science: Measurement, remote sensing, microphysics and modeling* (pp. 305–332). Elsevier. https://doi.org/10.1016/B978-0-12-822973-6.00008-1

Levizzani, V., Laviola, S., & Cattani, E. (2011). Detection and measurement of snowfall from space. *Remote Sensing*, *3*(1), 145–166. https://doi.org/10.3390/rs3010145

Lindstrom, E. J., Edson, J. B., Schanze, J. J., & Shcherbina, A. Y. (2019). SPURS-2: Salinity processes in the upper-ocean regional study 2 - The eastern equatorial Pacific experiment. *Oceanography*, *32*(2), 15–19. https://doi.org/10.5670/oceanog.2019.207

Lindstrom, E. J., Shcherbina, A. Y., Rainville, L., Farrar, J. T., Centurioni, L. R., Dong, S., et al. (2017). Autonomous multi-platform observations during the salinity processes in the upper-ocean regional study. *Oceanography*, *30*(2), 38–48. https://doi.org/10.5670/oceanog.2017.218

Lukas, R., & Lindstrom, E. (1991). The mixed layer of the western equatorial Pacific Ocean. *Journal of Geophysical Research*, *96*(S01), 3343–3357. https://doi.org/10.1029/90JC01951

Ma, B. B., & Nystuen, J. A. (2005). Passive acoustic detection and measurement of rainfall at sea. *Journal of Atmospheric and Oceanic Technology*, *22*(8), 1225–1248. https://doi.org/10.1175/JTECH1773.1

Maggioni, V., Meyers, P. C., & Robinson, M. D. (2016). A review of merged high-resolution satellite precipitation product accuracy during the Tropical Rainfall Measuring Mission (TRMM) era. *Journal of Hydrometeorology*, *17*(4), 1101–1117. https://doi.org/10.1175/JHM-D-15-0190.1

Nguyen, P., Ombadi, M., Afzali Gorooh, V., Shearer, E. J., Sadeghi, M., Sorooshian, S., et al. (2020a). PERSIANN dynamic Infrared-Rain Rate (PDIR-Now): A near-real-time quasi-global satellite precipitation dataset. *Journal of Hydrometeorology*, *21*(12), 2893–2906. https://doi.org/10.1175/JHM-D-20-0177.1

Nguyen, P., Shearer, E. J., Ombadi, M., Afzali Gorooh, V., Hsu, K., Sorooshian, S., et al. (2020b). PERSIANN Dynamic Infrared-Rain Rate Model (PDIR) for high-resolution, real-time satellite precipitation estimation. *Bulletin of the American Meteorology Society*, *101*(3), E286–E302. https://doi.org/10.1175/BAMS-D-19-0118.1

Nystuen, J. A. (2001). Listening to raindrops from underwater: An acoustic distrometer. *Journal of Atmospheric and Oceanic Technology*, *18*(10), 1640–1657. https://doi.org/10.1175/1520-0426(2001)018<1640:LTRFUA>2.0.CO;2

Ollitrault, M., & Colin de Verdière, A. (2014). The ocean general circulation near 1000-m depth. *Journal of Physical Oceanography*, *44*(1), 384–409. https://doi.org/10.1175/JPO-D-13-030.1

Petkovic, V., Orescanin, M., Kirstetter, P., Kummerow, C., & Ferraro, R. (2019). Enhancing PMW satellite precipitation estimation: Detecting convective class. *Journal of Atmospheric and Oceanic Technology*, *36*(12), 2349–2363. https://doi.org/10.1175/JTECH-D-19-0008.1

Prakash, S., Mahesh, C., & Gairola, R. M. (2012). Observed relationship between surface freshwater flux and salinity in the North Indian Ocean. *Atmospheric and Ocean Science Letters*, *5*(3), 163–169. https://doi.org/10.1080/16742834.2012.11446984

Prakash, S., Ramesh Kumar, M. R., Mathew, S., & Venkatesan, R. (2018). How accurate are satellite estimates of precipitation over the north Indian Ocean? *Theoretical and Applied Climatology*, *134*(1–2), 467–475. https://doi.org/10.1007/s00704-017-2287-2

Ramesh Kumar, M., & Schulz, J. (2002). Analysis of freshwater flux climatology over the Indian Ocean using the HOAPS data. *Remote Sensing of Environment*, *80*(3), 363–372. https://doi.org/10.1016/s0034-4257(01)00302-9

Reverdin, G., Supply, A., Drushka, K., Thompson, E. J., Asher, W. E., & Lourenco, A. (2020). Intense and small freshwater pools from rainfall investigated during SPURS-2 on November 9 2017 in the eastern tropical Pacific. *Journal of Geophysical Research: Oceans*, *125*(2), e2019JC015558. https://doi.org/10.1029/2019JC015558

Riser, S. C., Nystuen, J. A., & Rogers, A. (2008). Monsoon effects in the Bay of Bengal inferred from profiling float-based measurements of wind speed and rainfall. *Limnology & Oceanography*, *53*(5), 2080–2093. https://doi.org/10.4319/lo.2008.53.5_part_2.2080

Roemmich, D., Alford, M. H., Claustre, H., Johnson, K. S., King, B., Moum, J., et al. (2019). On the future of Argo: A global, full-depth, multi-disciplinary array. *Frontiers in Marine Science*, *6*, 439. https://doi.org/10.3389/fmars.2019.00439

Sapiano, M. R. P., & Arkin, P. A. (2009). An intercomparison and validation of high-resolution satellite precipitation estimates with 3-hourly gauge data. *Journal of Hydrometeorology*, *10*(1), 149–166. https://doi.org/10.1175/2008JHM1052.1

Schwartz, C. (2017). A comparison of methods used to populate neighborhood-based contingency tables for high-resolution forecast verification. *Weather and Forecasting*, *32*(2), 733–741. https://doi.org/10.1175/WAF-D-16-0187.1

Skofronick-Jackson, G. M., Johnson, B. T., & Munchak, S. J. (2013). Detection thresholds of falling snow from satellite-borne active and passive sensors. *IEEE Transactions on Geoscience and Remote Sensing*, *51*(7), 4177–4189. https://doi.org/10.1109/TGRS.2012.2227763

Sprintall, J., & Tomczak, M. (1992). Evidence of the barrier layer in the surface layer of the tropics. *Journal of Geophysical Research*, *97*(C5), 7305–7316. https://doi.org/10.1029/92JC00407

Tan, J., Huffman, G. J., Bolvin, D. T., & Nelkin, E. J. (2019). IMERG V06: Changes to the morphing algorithm. *Journal of Atmospheric and Oceanic Technology*, *36*(12), 2471–2482. https://doi.org/10.1175/JTECH-D-19-0114.1

Tan, J., Petersen, W. A., Kirstetter, P.-E., & Tian, Y. (2017). Performance of IMERG as a function of spatiotemporal scale. *Journal of Hydrometeorology*, *18*(2), 307–319. https://doi.org/10.1175/JHM-D-16-0174.s1

Thompson, E. J., Chen, H., Yang, J., & Bytheway, J. L. (2023). *High-resolution precipitation and wind measurements from passive aquatic listeners (PALs)*. NASA Global Hydrometeorology Resource Center DAAC. https://doi.org/10.5067/GPMGV/PAL/DATA101

Thompson, E. J., Moum, J. N., Rutledge, S. A., & Fairall, C. W. (2019). Wind limits on stable rain layers and diurnal warm layers throughout the MJO. *Journal of Geophysical Research: Oceans*, *124*(2), 897–924. https://doi.org/10.1029/2018JC014130

Trenberth, K., Smith, E. L., Qian, T., Dai, A., & Fasullo, J. (2007). Estimates of the global water budget and its annual cycle using observational and model data. *Journal of Hydrometeorology*, *8*(4), 758–769. https://doi.org/10.1175/JHM600.1

Wolff, D. B., & Fisher, B. L. (2008). Comparisons of instantaneous TRMM Ground validation and satellite rain-rate estimates at different spatial scales. *Journal of Applied Meteorology and Climatology*, *47*(8), 2215–2237. https://doi.org/10.1175/2008JAMC1875.1

Wu, Q., & Wang, Y. (2019). Comparison of oceanic multisatellite precipitation data from Tropical Rainfall Measurement Mission and Global Precipitation Measurement Mission datasets with rain gauge data from ocean buoys. *Journal of Atmospheric and Oceanic Technology*, *36*(5), 903–920. https://doi.org/10.1175/JTECH-D-18-0152.1

Xie, P., Joyce, R., Wu, S., Yoo, S.-H., Yarosh, Y., Sun, F., & Lin, R. (2017). Reprocessed, bias-corrected CMORPH global high resolution precipitation estimates from 1998. *Journal of Hydrometeorology*, *18*(6), 1617–1641. https://doi.org/10.1175/JHM-D-16-0168.1

Xie, P., Joyce, R., Wu, S., Yoo, S.-H., Yarosh, Y., Sun, F., et al. (2019). *NOAA climate data record (CDR) of CPC morphing technique (CMORPH) high resolution global precipitation estimates, version 1 [30 min, 8km]*. NOAA National Centers for Environmental Information. https://doi.org/10.25921/w9va-q159

Yang, J., Riser, S. C., Nystuen, J. A., Asher, W. E., & Jessup, A. T. (2015). Regional rainfall measurements using the Passive Aquatic Listener during the SPURS field campaign. *Oceanography*, *28*(1), 124–133. https://doi.org/10.5670/oceanog.2015.10